

# AN INVERSE PROBLEM FOR THE ONE-PHASE STEFAN PROBLEM WITH VARYING MELTING TEMPERATURE

MARC DAMBRINE AND HELMUT HARBRECHT

**ABSTRACT.** The present article is dedicated to the forward and backward solution of a transient one-phase Stefan problem. In the forward problem, we compute the evolution of the initial domain for a Stefan problem where the melting temperature varies over time. This occurs in practice, for example, when the pressure in the external space changes in time. In the corresponding backward problem, we then reconstruct the time-dependent melting temperature from the knowledge of the evolving geometry. We develop respective numerical algorithms using a moving mesh finite element method and provide numerical simulations.

## 1. INTRODUCTION

**1.1. Stefan problem.** The classic Stefan problem dates back to Josef Stefan in 1889, who studied ice formation in the polar seas, see [22]. He discovered that this growth problem is related to heat problems in which not only the temperature, which is the solution of a partial differential equation, is unknown but also the position of the surface moves over time and is therefore part of the problem.

This particular problem belongs to the class of problems with moving boundaries. In general, such problems contain time-dependent boundaries that are unknown and depend on temporal and spatial variables. Problems with moving boundaries are also referred to as Stefan problems. This contrasts with problems with free boundary. The latter also contain boundaries that are unknown in advance, but these boundaries are in a steady state and are therefore not time-dependent, cf. [6].

There is a wealth of literature on the Stefan problem, see [10, 12, 18, 20, 23] for example and the references contained therein. This literature deals mainly with the analysis of the Stefan problem. Stefan problems arise, for example, in the modelling of phase transitions, chemical reactions, fluid flows in porous media or the melting of ice, compare [6].

When solving a Stefan problem numerically, one encounters the problem of handling the moving boundary. In [6], various numerical methods are explained, compare also [11, 16] and the references therein: front tracking methods, front fixing methods,

and fixed domain methods. Front tracking methods calculate the position of the moving boundary at each time step. Front fixing methods attempt to fix the front by choosing a suitable spatial coordinate system. In fixed domain methods, the problem is reformulated, for example using the enthalpy method, so that the position of the boundary appears as a feature of the solution, see [6]. Note that also shape optimization can be used to compute directly the evolving surface of the Stefan problem, compare [3, 17].

**1.2. Motivation and background.** As part of a recent collaboration with physicists, we looked in [21] at the growth and melting of methane hydrates. The experiment involved changing the pressure inside a capillary tube in which such a hydrate crystal grows in the presence of two components: water and methane gas dissolved in it. The growth or melting of the crystal was filmed and the rate of gas dissolved in the liquid part was measured by Raman spectrometry.

The conclusion of the study [21] is that the dynamics of the boundary and the gas concentrations measured are consistent with a two-phase Stefan model, in which the melting temperature at the interface between the hydrate and the aqueous phase is not the melting temperature of the hydrate single crystal. To reach this conclusion, we used, in the one-dimensional framework of the capillary experiments, analytical formulas giving the evolution of the front as a function of this temperature at the melting front. The experimental observation focused on the dynamics of the front, and an explicit formula was used to determine the temperature at the front.

In this article, we ask the following general question, which generalizes the previous situation in a context where we do not have analytical formulas: is it possible to determine the melting temperature from observations of the evolution of the free surface? This melting temperature depends in particular on pressure. To limit the number of experiments required, the idea would be to vary this pressure slowly in the experimental setup. To do this, we must consider a transient version of Stefan's problem.

The specific question we are considering in this article is therefore the following: if we observe the evolution of a free boundary evolving according to a Stefan model in which the temperature at the interface between phases varies with time, is it possible to reconstruct the melting temperature as a function of time?

**1.3. Our contribution.** Answering the above question in a general context would be ambitious and is not the objective of this article. We wish to conduct a preliminary study and respond from a numerical perspective to the feasibility of this problem in

a proof-of-concept spirit. That is why we will place ourselves in the simplest non-trivial framework possible: the evolution of a star-shaped domain in two dimensions.

For the direct problem, we consider a single-phase Stefan problem where the temperature imposed at the boundary is given and depends on time. The inverse problem is then as follows: suppose we know the evolution of a domain governed by a Stefan model with a temperature that varies over time. Can we reconstruct the melting temperature?

**1.4. Content.** This article is organized as follows. First, in Section 2, we introduce notation and specify the transient Stefan problem that we are considering. The numerical method that we propose for solving the problem under consideration is presented on Section 3. Specifically, we employ a finite element method to solve the heat equation in combination with a front tracking method. Section 4 is then concerned with the inverse problem. We discuss necessary conditions for identifiability and propose some related positive and negative examples. We then present numerical experiments that demonstrate that monitoring of the free boundary enables the determination of the varying temperature at the front. Finally, we state concluding remarks in Section 5.

## 2. A NONSTATIONARY STEFAN PROBLEM

**2.1. Classical one-phase Stefan problem.** Let us consider the classical one-phase Stefan problem as described in [13]. This specific Stefan problem models the evolution of the solid-liquid phase interface. Thus, for every point of time  $t \in [0, T]$ , we have a time-dependent spatial domain which we denote by  $\Omega_t \subset \mathbb{R}^d$ ,  $d \geq 2$ . This spatial domain has a time-dependent spatial boundary  $\Gamma_t := \partial\Omega_t$ . By setting

$$(1) \quad Q_T = \bigcup_{0 < t < T} (\{t\} \times \Omega_t),$$

we obtain the space-time non-cylindrical domain (also called *space-time tube*) with lateral boundary

$$\Sigma_T = \bigcup_{0 < t < T} (\{t\} \times \Gamma_t).$$

The setup is illustrated in Figure 1 for two spatial dimensions plus the temporal dimension.

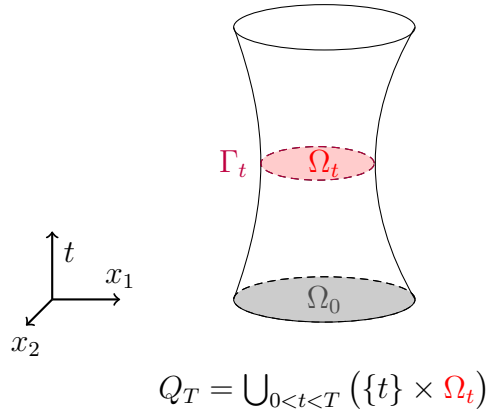


FIGURE 1. Geometric setup of the Stefan problem: The space-time tube  $Q_T$  is given by the time-evolution of the initial domain  $\Omega_0$ . The cut area at time  $t$  is the domain  $\Omega_t$  with boundary  $\Gamma_t = \partial\Omega_t$ .

For the formulation of the one-phase Stefan problem, we follow [13, 14]. The temperature  $u(t, \mathbf{x})$  of the liquid in  $\Omega_t$  is thus described by the partial differential equation

$$(2) \quad \partial_t u - \Delta u = 0 \quad \text{in } \Omega_t,$$

$$(3) \quad \langle \mathbf{V}, \mathbf{n} \rangle = -\frac{\partial u}{\partial \mathbf{n}} \quad \text{on } \Gamma_t,$$

$$(4) \quad u = u_m \quad \text{on } \Gamma_t,$$

$$(5) \quad u(0, \cdot) = u_0 \quad \text{in } \Omega_0 = \Omega.$$

We assume throughout this article, that the Dirichlet data match the initial condition, meaning that  $u(0, \mathbf{x}) = u_m$  for all  $\mathbf{x} \in \Gamma_0$ .

The domain  $\Omega$  in (5) is the initial shape of the liquid phase while condition (3) is called the Stefan condition [14]. It comes from the movement of the phase interface, see [24, pg. 387]. The Stefan condition expresses that the normal velocity  $\langle \mathbf{V}, \mathbf{n} \rangle$  of the surface  $\Gamma_t$  equals minus the normal derivative of  $u$  at the boundary. We prescribe the initial position of the interface and the initial temperature distribution to make the problem meaningful. From this Stefan problem, we can see that the liquid freezes at zero temperature, cf. [13]. Notice that the one-phase Stefan problem is actually also a two-phase Stefan problem, but the temperature is only unknown in one region, while it is equal to  $u_m$  in the other region, compare [24].

The domain  $\Omega_t$ , thus the region which contains the liquid phase, is characterized by  $\{\mathbf{x} \in \mathbb{R}^d : u(t, \mathbf{x}) > u_m\}$  if we have  $u_0 > u_m$  in  $\Omega$ . Therefore,  $u$  can be interpreted as a level set function. Due to (2), the parabolic Hopf lemma (see e.g. [9] for some remarks) implies  $\partial u / \partial \mathbf{n} < 0$  on  $\Gamma_t$  for  $t > 0$ . Therefore, we obtain the so-called

*Rayleigh-Taylor sign condition*

$$-\frac{\partial u_0}{\partial \mathbf{n}} \geq \lambda > 0 \text{ on } \Gamma_0,$$

which ensures the nondegeneracy in accordance with [13]. Vice versa, when  $u_0 < u_m$  in  $\Omega$ , we find  $\partial u / \partial \mathbf{n} < 0$  on  $\Gamma_t$  for  $t > 0$  and hence

$$-\frac{\partial u_0}{\partial \mathbf{n}} \leq \lambda < 0 \text{ on } \Gamma_0.$$

**2.2. Varying the melting temperature.** The melting temperature in the classical Stefan problem (2)–(5) is fixed. In contrast, we consider in the present article the situation that the melting temperature  $u_m = u_m(t)$  varies over time and is thus time-dependent. In practice, this can be achieved by changing the pressure in the external space during time.

In order to solve the Stefan problem (2)–(5) with time-dependent melting temperature, we make the ansatz  $v = u - u_m$ . In view of  $\Delta u_m = 0$ , this amounts to

$$(6) \quad \partial_t v - \Delta v = -\dot{u}_m \quad \text{in } \Omega_t,$$

$$(7) \quad \langle \mathbf{V}, \mathbf{n} \rangle = -\frac{\partial v}{\partial \mathbf{n}} \quad \text{on } \Gamma_t,$$

$$(8) \quad v = 0 \quad \text{on } \Gamma_t,$$

$$(9) \quad v(0, \cdot) = v_0 \quad \text{in } \Omega_0 = \Omega,$$

where we set  $v_0 := u_0 - u_m(0)$ .

In the following, we will solve the transformed problem (6)–(9) rather than the original problem (2)–(5). The solution  $u$  of the latter is then obtained in accordance with  $u = v + u_m$ .

**2.3. Generation of the space-time tube.** In order to generate a space-time tube, we can adopt two different points of view. For both of them, let us assume that we have a spatial domain  $\Omega_{\text{ref}}$ , which serves as reference domain. One can generate a space-time tube  $Q_T$  by mapping this domain  $\Omega_{\text{ref}}$  to a spatial domain  $\Omega_t$  for every point of time  $t$ , see also Figure 1.

On the one hand, this can be done by considering a velocity field  $\mathbf{V}$  and associate to it the solution  $\mathbf{T}(t, \cdot) : \mathbf{x} \mapsto \mathbf{x}_t = \mathbf{T}(t, \mathbf{x})$  of the differential equation

$$(10) \quad \begin{aligned} \frac{\partial}{\partial t} \mathbf{T}(t, \mathbf{x}) &= \mathbf{V}(t, \mathbf{T}(t, \mathbf{x})) & \text{in } (0, T) \times \Omega_{\text{ref}}, \\ \mathbf{T}(0, \mathbf{x}) &= \mathbf{T}_0(\mathbf{x}) & \text{in } \Omega_{\text{ref}}, \end{aligned}$$

see [26, pg. 6] or [19] for the details. The map  $\mathbf{T}(t, \cdot)$  thus describes the pathline of an individual particle being exposed to the velocity field  $\mathbf{V}$ . By setting  $\Omega_t = \mathbf{T}(t, \Omega_{\text{ref}})$ , we finally generate the space-time tube  $Q_T$ , see Figure 2 for an illustration.

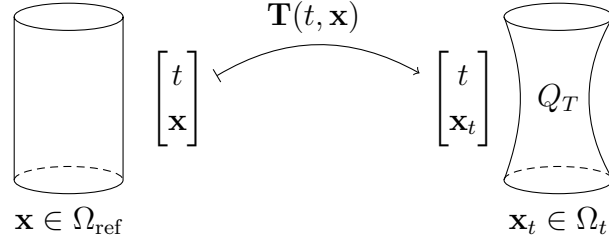


FIGURE 2. Generation of the space-time tube by the mapping  $\mathbf{T}(t, \cdot)$  induced by the velocity field  $\mathbf{V}$ . In particular, the relation  $\Omega_t = \mathbf{T}(t, \Omega_{\text{ref}})$  always applies.

**2.4. Solution algorithm for the transient Stefan problem.** In order to derive an algorithm for the transient Stefan problem (6)–(9), we choose a small time step  $\Delta t$  and set  $t_k := k\Delta t$  for  $k \in \mathbb{N}_0$ . We then aim at approximating the domains  $\Omega_k := \Omega_{t_k}$  and hence the mappings  $\mathbf{T}_k := \mathbf{T}(t_k, \cdot)$  for all  $k \in \mathbb{N}$ .

To this end, we solve successively the heat equation for each time interval  $t \in [t_k, t_{k+1}]$  on the fixed domain  $\Omega_k$ . This means, we consider the time slice  $[t_k, t_{k+1}] \times \Omega_k$  and solve the initial boundary value problem

$$(11) \quad \partial_t \tilde{v} - \Delta \tilde{v} = -\dot{u}_m \quad \text{in } \Omega_k,$$

$$(12) \quad \tilde{v} = 0 \quad \text{on } \Gamma_k,$$

$$(13) \quad \tilde{v}(t, \cdot) = v_k \quad \text{in } \Omega_k,$$

where  $v_k$  is the solution from the previous time step at time  $t_k$ . After having the solution  $\tilde{v}$  at hand, we can use the Stefan condition (7) to update the boundary of the (approximate) space-time tube in accordance with

$$(14) \quad \Gamma_{k+1} := \left\{ \mathbf{x} - \Delta t \frac{\partial \tilde{v}}{\partial \mathbf{n}}(t_{k+1}, \mathbf{x}) \mathbf{n}(\mathbf{x}) : \mathbf{x} \in \Gamma_k \right\}.$$

This defines the new domain  $\Omega_{k+1}$  and thus the map  $\mathbf{T}_{k+1}$ . The new initial data  $v_{k+1}$ , entering the computation of  $\tilde{v}$  in the next time slice  $[t_{k+1}, t_{k+2}] \times \Omega_{k+1}$ , are obtained by interpolating the solution  $\tilde{v}$  of (11)–(13) at time  $t = t_{k+1}$  onto the updated domain  $\Omega_{k+1}$ . Hence, we especially have the identity

$$v_{k+1}(\mathbf{x}) := \tilde{v}(t_{k+1}, \mathbf{x}) \quad \text{for all } \mathbf{x} \in \Omega_k \cap \Omega_{k+1}.$$

Having the new initial data  $v_{k+1}$  and the updated domain  $\Omega_{k+1}$  at hand, we can repeat the above procedure to compute  $\tilde{v}$  on the next time slice  $[t_{k+1}, t_{k+2}] \times \Omega_{k+1}$ . Since we track the boundary of the sought space-time cylinder  $Q_T$ , associated with the transient Stefan problem (2)–(5), the proposed method belongs to the class of front tracking methods.

### 3. NUMERICAL SIMULATION OF THE FORWARD SOLUTION

**3.1. Discretization of the space-time tube.** The key ingredient of any numerical method to solve the transient Stefan problem (2)–(5) is the discretization of the sought space-time tube  $Q_T$ . As we approximate it by a piecewise constant function in time through the approximations of the time slices  $[t_k, t_{k+1}] \times \Omega_k$ ,  $k \in \mathbb{N}_0$ , we only need to discretize the domain  $\Omega_k$ , which is considered in the following.

Under the assumption that the domain  $\Omega_k$  is star-shaped, we can represent its boundary by means of a Fourier series. We hence can make the ansatz

$$(15) \quad \Gamma_k := \left\{ \left( a_{k,0} + \sum_{\ell=1}^M [a_{k,\ell} \cos(\ell\varphi) + a_{k,-\ell} \sin(\ell\varphi)] \right) \begin{bmatrix} \cos(\varphi) \\ \sin(\varphi) \end{bmatrix} : \varphi \in [0, 2\pi] \right\},$$

which identifies the domain  $\Omega_k$  (respectively its boundary  $\Gamma_k$ ) with the  $2M + 1$  Fourier coefficients

$$\mathbf{a}_k = [a_{k,-M}, \dots, a_{k,-1}, a_{k,0}, a_{k,1}, \dots, a_{k,M}] \in \mathbb{R}^{2M+1}$$

of the representation of its boundary  $\Gamma_k$ .

If we define the reference domain  $\Omega_{\text{ref}}$  as the unit disc, that is

$$\Omega_{\text{ref}} := \{ \mathbf{x} \in \mathbb{R}^2 : \|\mathbf{x}\|_2 < 1 \}.$$

we obtain for the associated domain  $\Omega_k$  the mapping  $\mathbf{T}_k$  by

$$(16) \quad \mathbf{T}_k : \Omega_{\text{ref}} \rightarrow \Omega_k, \quad \mathbf{T}_k(\mathbf{x}) = \left( a_{k,0} + \sum_{\ell=1}^M [a_{k,\ell} \cos(\ell\hat{\mathbf{x}}) + a_{k,-\ell} \sin(\ell\hat{\mathbf{x}})] \right) \mathbf{x}.$$

Herein, the expression

$$\hat{\mathbf{x}} := \frac{\mathbf{x}}{\|\mathbf{x}\|}$$

denotes the radial direction, which is interpreted as the polar angle in the series expansion.

We refer to Figure 3 for an illustration of our construction of the mapping  $\mathbf{T}_k$  including finite element meshes on  $\Omega_{\text{ref}}$  and on the given domain  $\Omega_k$ . Note that the finite element mesh on  $\Omega_k$  is obtained by mapping the finite element mesh on  $\Omega_{\text{ref}}$  by using  $\mathbf{T}_k$ . Note that the boundary vertices of the mesh on the unit disc  $\Omega_{\text{ref}}$  are

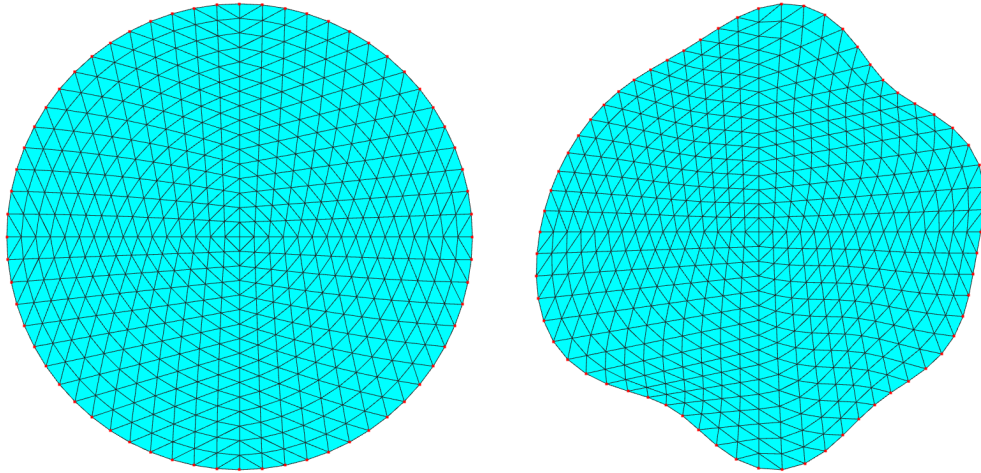


FIGURE 3. The finite element mesh on the circle and its mapped counterpart on the deformed domain  $\Omega_k$ .

equidistant which ensures that the boundary vertices of the mesh on the mapped domain  $\Omega_k$  are always equidistant with respect to the polar angle. This enables the application of the fast Fourier transform [5] to speed up the computations in the following.

**3.2. Discretization of the heat equation.** In order to solve the heat equation (11)–(13) in a given time slice  $[t_k, t_{k+1}] \times \Omega_k$ , we apply the finite element method. To this end, we compute a mesh by mapping a given quasi-uniform mesh of the unit circle  $\Omega_{\text{ref}}$  to the actual domain  $\Omega_k$  by application of the mapping  $\mathbf{T}_k$  from (16). Note that this mesh mapping method ensures that we always have the same mesh with vertices that are transported by  $\mathbf{T}_k$ .

For sake of simplicity, we assume that the melting temperature  $u_m(t)$  is piecewise linear in each time interval  $[t_k, t_{k+1}]$ . Then, given the domain  $\Omega_k$  in the  $(k+1)$ -st time step, we consider a quasi-uniform mesh (computed as described above) and the associated finite element space  $V_k = \text{span}\{\varphi_i : i = 1, \dots, N\}$ , consisting of  $N$  piecewise linear Lagrangian finite element basis functions  $\{\varphi_i\}_i$ . We define the finite element stiffness and mass matrices

$$\mathbf{A}_k = [(\nabla \varphi_i, \nabla \varphi_j)_{L^2(\Omega_k)}]_{i,j=1}^N, \quad \mathbf{M}_k = [(\varphi_i, \varphi_j)_{L^2(\Omega_k)}]_{i,j=1}^N,$$

as well as the right-hand side

$$\mathbf{f}_k = [(1, \varphi_j)_{L^2(\Omega_k)}]_{i=1}^N,$$

compare [1, 2] for example. Then, the finite element function

$$v_{k+1} = \sum_{i=1}^N v_{k+1,i} \varphi_i \in V_k$$

is given by using the trapezoidal rule in time as the solution of the following linear system of equations

$$(17) \quad \left( \mathbf{M}_k + \frac{\Delta t}{2} \mathbf{A}_k \right) \mathbf{v}_{k+1} = \left( \mathbf{M}_k - \frac{\Delta t}{2} \mathbf{A}_k \right) \mathbf{v}_k - \Delta t \alpha_k \mathbf{f}_k.$$

Herein,  $\alpha_k$  denotes the derivative of the melting temperature  $u_m(t)$  in the interval  $[t_k, t_{k+1}]$ . We emphasize  $\alpha_k$  can be replaced by an appropriate constant approximation of  $\dot{u}_m$  if the melting temperature  $u_m(t)$  is not linear in the time interval  $[t_k, t_{k+1}]$ . In the context of finite element methods, the discretization underlying the system (17) is also known as Crank-Nicolson method, introduced in [7] and being second order accurate in space and time.

**3.3. Updating the domain.** Having the finite element solution  $v_{k+1}$  for the time step  $t_{k+1}$  at hand, we can compute the update of the domain  $\Omega_k$ . To this end, we note that the gradient of  $v_{k+1}$  at the boundary  $\Gamma_k$  is given by

$$\nabla v_{k+1}(\mathbf{x}) = \frac{\partial v_{k+1}}{\partial \mathbf{n}}(\mathbf{x}) \mathbf{n}(\mathbf{x}),$$

since the tangential derivative  $(\partial v_{k+1} / \partial \mathbf{t})(\mathbf{x}) = 0$  vanishes for all  $\mathbf{x} \in \Gamma_k$  due to the homogenous Dirichlet data. Therefore, we can update the boundary in radial direction by using the modified Stefan condition

$$-\langle \mathbf{V}, \hat{\mathbf{x}} \rangle = \langle \nabla v_{k+1}, \hat{\mathbf{x}} \rangle = \frac{\partial v_{k+1}}{\partial \mathbf{n}} \langle \mathbf{n}, \hat{\mathbf{x}} \rangle \quad \text{on } \Gamma_k.$$

We hence have to update all points on the boundary in the radial direction by means of the formula

$$(18) \quad \mathbf{x}_{k+1} := \mathbf{x} - \Delta t \frac{\partial v_{k+1}}{\partial \mathbf{n}} \langle \mathbf{n}, \hat{\mathbf{x}} \rangle \hat{\mathbf{x}} \quad \text{on } \Gamma_k.$$

In our numerical method, we realize the update (18) as follows. Under the assumption that the vertices of the mesh on the boundary correspond to an equidistant subdivision of the radial function with respect to the polar angle, we can apply the fast Fourier transform to compute the update of the coefficients in the Fourier series. However, there are typically more vertices on the boundary than Fourier coefficients in the representation (15). Therefore, we always truncate the update to its  $2M + 1$  leading coefficients which corresponds to a least squares fit of the new parametrization using the  $2M + 1$  Fourier coefficients.

In a final step, the finite element function  $v_{k+1}$ , given on the old domain  $\Omega_k$ , is interpolated onto the updated domain  $\Omega_{k+1}$  by means of kernel interpolation. Kernel interpolation is a very efficient approach for scattered data interpolation, see [8, 25] for example. In our implementation, we use the exponential kernel  $\kappa(\mathbf{x}, \mathbf{y}) = \exp(-\|\mathbf{x} - \mathbf{y}\|_2)$  for the interpolation, which results in an interpolation error that is known to converge in the  $L^2$ -norm with order  $h^{-2}$ .

In order to explain the kernel interpolation method, let  $\{\mathbf{y}_{k,i}\}_i$  denote the vertices of the finite element mesh on  $\Omega_k$  and let  $v_{k+1}^{\text{old}} \in V_k$  be the finite element function  $v_{k+1}$  which comes from the solution of (17). Assuming that there are  $L$  vertices, we define the  $L \times L$  kernel matrices

$$\mathbf{K} = [\kappa(\mathbf{y}_{k,i}, \mathbf{y}_{k,j})]_{i,j=1}^L, \quad \mathbf{L} := [\kappa(\mathbf{y}_{k,i}, \mathbf{y}_{k+1,j})]_{i,j=1}^L.$$

Then, the finite element function  $v_{k+1}^{\text{new}} \in V_{k+1}$  with respect to the new vertices  $\{\mathbf{y}_{k+1,i}\}_i$  is given through the nodal values obtained from

$$\mathbf{v}^{\text{new}} = \mathbf{L} \mathbf{K}^{-1} \mathbf{v}^{\text{old}}, \quad \text{where } \mathbf{v}^{\text{old}} = [v_{k+1}^{\text{old}}(\mathbf{y}_{k,i})]_{i=1}^L.$$

This means that there holds  $v_{k+1}^{\text{new}}(\mathbf{y}_{k+1,i}) = [\mathbf{v}^{\text{new}}]_i$  for all new vertices  $\mathbf{y}_{k+1,i}$ ,  $i = 1, \dots, L$ . We refer to [8, 25] for further details.

**3.4. Numerical results of the forward simulation.** We shall present some numerical tests. We consider the time interval  $[0, 5]$ , that is  $T = 5$ , and set  $\Delta t = 5/100$ , which results in 100 time steps. We apply  $2M + 1 = 29$  Fourier coefficients in the Fourier series of the radial function in the boundary representation (15). The finite element mesh we use consists of about 16000 finite elements, leading to about  $N = 8000$  piecewise linear Lagrangian finite element basis functions. We prescribe the melting temperature  $u_m(t) = 1/20(t - 5/2)^2$  in the first example while it is set as  $u_m(t) = 1/20(\cos(2t) - 1)$  in the second example. The initial domain is chosen randomly in both simulations and the initial temperature has been set to be constant, which means  $u_0 := u_m(0)$ . The simulations run quite fast and the computed space-time tubes are found in Figure 4 for the first example and in Figure 5 for the second example.

In the first example, the domain grows for  $t \in [0, 5/2]$ , becoming more and more a circle. Then, it shrinks again for  $t \in [5/2, 5]$ , compare Figure 4. This is due to the increase of the melting temperature in the time interval  $[0, 5/2]$  and the decrease of the melting temperature in the time interval  $[5/2, 5]$ . We observe especially that the final boundary is close to the boundary of the initial domain.

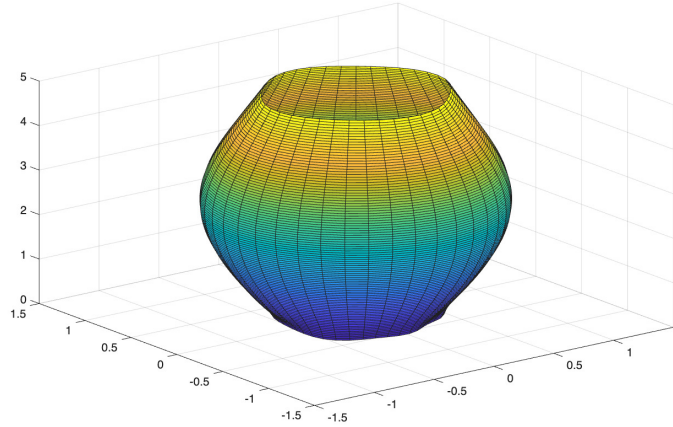


FIGURE 4. The space-time tube in case of the melting temperature  $u_m(t) = 1/20(t - 5/2)^2$ .

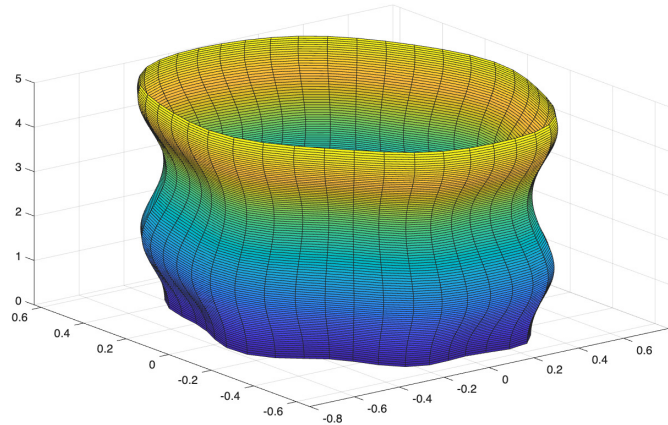


FIGURE 5. The space-time tube in case of the melting temperature  $u_m(t) = 1/20(\cos(2t) - 1)$  on the right.

In the second example, the shape oscillates around the initial shape, while the shape of the surface becomes smoother and smoother over time, compare Figure 5. Indeed, the evolving boundary tends towards a disc. The reason for this is that the initial domain does not grow so much in comparison to the first example, so that it changes its shape only slightly.

#### 4. INVERSE RECONSTRUCTION

**4.1. On necessary conditions for the identifiability.** We shall next consider the *inverse problem*, namely the reconstruction of the melting temperature from measurements of the evolving surface.

The melting temperature appears as the Dirichlet trace of the temperature on the surface of the space-time tube. If the space-time tube is known, the deformation velocity of its surface is also known. Thus, if the space-time tube in question corresponds to Stefan's dynamics, the inverse problem of reconstructing the melting temperature is easy to solve. We should, however, take a closer look on the identifiability.

Consider a given domain tube  $Q_T$ , given as in (1), which has been generated by Stefan's dynamics. In a first step, it suffices to solve the Neumann problem for the heat equation on  $Q_T$ , with Neumann data corresponding to the (negative) normal speed of deformation of the domain tube:

$$\begin{aligned} \partial_t u - \Delta u &= 0 && \text{in } \Omega_t, \\ \frac{\partial u}{\partial \mathbf{n}} &= -\langle \mathbf{V}, \mathbf{n} \rangle && \text{on } \Gamma_t, \\ u(0, \cdot) &= u_0 && \text{in } \Omega_0 = \Omega. \end{aligned}$$

This problem has already been studied, notably in the article of Hofmann and Lewis [15] who established the existence and uniqueness of a solution to this problem under certain assumptions of regularity of the tube (see also the article of Brügger et al. in [4] for an integral equation resolution). Then, in a second step, we must take the Dirichlet trace, which is necessarily the function to be reconstructed.

This procedure can, of course, be applied to any sufficiently regular space-time tube  $Q_T$ , even if it does not correspond to a Stefan-type evolution. The criterion that distinguishes the two cases is as follows: the trace of the solution to the heat equation on the space-time tube with the Neumann condition must be a constant on the boundary of each section  $\Omega_t$  of the tube.

**Example 4.1.** *Let us consider the specific case of an disk*

$$\Omega_0 = \{\mathbf{x} : \|\mathbf{x}\|_2 < R_0\}$$

*as initial domain. The invariance of the problem with respect to rotations around the center of the disk implies that Stefan's dynamics generates a space-time tube  $Q_T$  whose sections  $\Omega_t$  are also disks. As a consequence, there are space-time tubes that do not correspond to Stefan's dynamics: Let  $\Omega_t$  be the ellipse with center at the origin that satisfies the equation*

$$\frac{x^2}{(1+t)^2} + \frac{y^2}{(1+2t)^2} = 1.$$

*Then, the initial section  $\Omega_0$  of the associated space-time tube  $Q_T$  is a disk, but the domains  $\Omega_t$  are not for  $t > 0$ .*

We next like to discuss whether the knowledge of the final domain  $\Omega_T$  allows us to reconstruct the temperature trajectory. To this end, let us consider a regular function  $t \mapsto R(t)$  with non-negative values and the tube

$$Q_T = \{(t, \mathbf{x}) : \|\mathbf{x}\|_2 < R(t), t \in [0, T]\}.$$

The solution  $u$  to the heat equation

$$\begin{aligned} \partial_t u - \Delta u &= 0 && \text{in } \Omega_t = \{\mathbf{x} : \|\mathbf{x}\|_2 < R(t)\}, \\ \frac{\partial u}{\partial \mathbf{n}} &= -R'(t) && \text{on } \Gamma_t, \\ u(0, \cdot) &= u_0 && \text{in } \Omega_0 = \Omega. \end{aligned}$$

is radial, and therefore the transient melting temperature is simply  $t \mapsto u(t, \mathbf{x}(t))$  with  $\|\mathbf{x}(t)\| = R(t)$ . As a consequence, we get

**Lemma 4.2.** *For any  $R_T > 0$  and for any final time  $T$ , there exists a temperature trajectory  $u_m(t)$  that transforms, through the Stefan dynamics, the initial disk into a disk with radius  $R_T$  at time  $T$ .*

The answer to the question of unique identifiability from knowledge of the final domain  $\Omega_T$  is thus clearly no. Consider the disk of radius  $R_0$  as initial domain and the disk of radius  $R_T$  as the final one at time  $T$ . For any  $R > 0$ , one can construct a Stefan tube such that  $\Omega_0 = \{\mathbf{x} : \|\mathbf{x}\|_2 < R_0\}$ ,  $\Omega_{T/2} = \{\mathbf{x} : \|\mathbf{x}\|_2 < R\}$  and  $\Omega_T = \{\mathbf{x} : \|\mathbf{x}\|_2 < T\}$  by the previous lemma.

Since it generally appears difficult to characterize the necessary condition theoretically in geometric terms on a space-time tube, we will instead conduct numerical simulations.

**4.2. Reconstruction of the melting temperature.** To reconstruct of the melting temperature from measurements of the evolving surface, we proceed as follows. For each time step  $k = 0, 1, 2, \dots$ , we solve (11)–(13) by setting  $u'_m := 1$ , meaning that we assume that the change of the melting temperature in the time-interval  $[t_k, t_{k+1}]$  is piecewise linear. Since the solution  $\tilde{v}$  of (11)–(13) depends linearly on the inhomogeneity  $-\dot{u}_m = -1$  and so does the flux, we can determine the scaling factor  $\alpha_k$  such that we match the measured boundary  $\Gamma_{k+1}$  by the update rule (14) best possible, meaning that we search for  $\alpha_k \in \mathbb{R}$  such that

$$(19) \quad \Gamma_{k+1} \stackrel{!}{=} \left\{ \mathbf{x} - \alpha_k \Delta t \frac{\partial \tilde{v}}{\partial \mathbf{n}}(t_{k+1}, \mathbf{x}) \mathbf{n}(\mathbf{x}) : \mathbf{x} \in \Gamma_k \right\}.$$

In that way, we can determine successively the time derivative  $\dot{u}_m$  of the melting temperature, leading to

$$\dot{u}_m(t) = \alpha_k, \quad \text{for all } t \in [t_k, t_{k+1}] \text{ and } k \in \mathbb{N}_0.$$

Therefore, by integrating this piecewise approximation with respect to the time, we obtain the sought melting temperature  $u_m$ .

The method to solve equation (19), which corresponds to a shape identification problem, is discussed in the next subsection. Especially, we investigate there the sensitivity of this reconstruction with respect to measurement errors by numerical tests.

**4.3. Setup and algorithm.** We now test our reconstruction algorithm proposed in the previous subsection. To that end, we consider the same two examples as in Section 3, but now try to reconstruct the melting temperature from the observed space-time tubes. To this end, we add (uncorrelated) random noise to the Fourier coefficients of the desired space-time tubes. The noise levels  $\delta$  under consideration are  $\delta = 0.25\%$ ,  $\delta = 0.5\%$ ,  $\delta = 1.0\%$ , and  $\delta = 2.0\%$ . Recall that the prescribed space-time tubes have been visualized in Figure 4 and Figure 5, respectively. Moreover, to avoid an inverse crime, we use only  $2M + 1 = 15$  Fourier coefficients for the reconstruction of the evolving boundary of the space-time tube and a coarser mesh for the finite element solver. It consists of about 2000 finite elements, which results in about  $N = 1000$  piecewise linear Lagrangian finite element basis functions.

The procedure for the reconstruction is as follows. In the  $(k + 1)$ -st time step, we take the Fourier series  $\mathbf{a}_k$  for granted to define the domain  $\Omega_k$ . We solve (11)–(13) for the right-hand side  $u'_m = 1$  and determine the scaling factor  $\alpha_k$  in such a way that the update (18) matches the desired boundary  $\mathbf{a}_{k+1}$ :

$$(20) \quad \mathbf{x}_{k+1}^{\text{desired}} \stackrel{!}{=} \mathbf{x} - \alpha_k \Delta t \frac{\partial v_{k+1}}{\partial \mathbf{n}} \langle \mathbf{n}, \hat{\mathbf{x}} \rangle \hat{\mathbf{x}} \quad \text{on } \Gamma_k.$$

Of course, this equation cannot be solved exactly. Hence, we solve it for all vertices of the finite element mesh that lie on the boundary in a least-squares sense.

**4.4. Numerical realization.** In the following, we discuss what the solution of (20) means in the context of our finite element discretization. In view of the linear system (17) of equations, we split the the discrete flux  $\frac{\partial v_{k+1}}{\partial \mathbf{n}}$  into the contribution  $\frac{\partial v_{k+1}^{(1)}}{\partial \mathbf{n}}$  arising from

$$\left( \mathbf{M}_k + \frac{\Delta t}{2} \mathbf{A}_k \right) \mathbf{v}_{k+1}^{(1)} = \left( \mathbf{M}_k - \frac{\Delta t}{2} \mathbf{A}_k \right) \mathbf{v}_k,$$

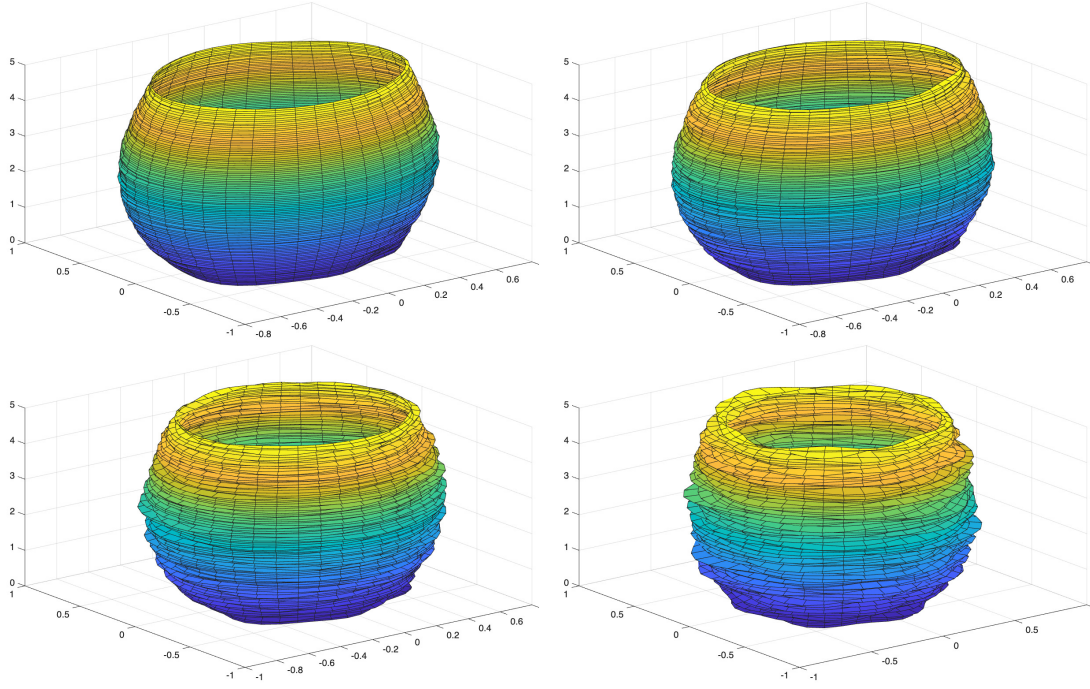


FIGURE 6. The reconstruction of the space-time tube in case of the first example with 0.25% random noise (top left), 0.5% random noise (top right), 1.0% random noise (bottom left), and 2.0% random noise (bottom right).

and the contribution  $\frac{\partial v_{k+1}^{(2)}}{\partial \mathbf{n}}$  arising from

$$\left( \mathbf{M}_k + \frac{\Delta t}{2} \mathbf{A}_k \right) \mathbf{v}_{k+1}^{(2)} = -\Delta t \mathbf{f}_k.$$

Recall that  $\{\mathbf{y}_{k,i}\}_i$  denote the vertices of the finite element mesh on  $\Omega_k$  and generate the desired vertices  $\{\mathbf{y}_{k+1,i}^{\text{desired}}\}_i$  given by the Fourier coefficients of the measurement for  $\Omega_{k+1}^{\text{desired}}$ . Since they are equidistant with respect to the polar angle, we can use the fast Fourier transform for this. Thus, the discrete version of (20) becomes

$$\alpha_k \frac{\partial v_{k+1}^{(2)}}{\partial \mathbf{n}}(\mathbf{y}_{k,i}) \langle \mathbf{n}, \mathbf{y}_{k,i} \rangle \mathbf{y}_{k,i} = \frac{\mathbf{y}_{k+1,i}^{\text{desired}} - \mathbf{y}_{k,i}}{\Delta t} - \frac{\partial v_{k+1}^{(1)}}{\partial \mathbf{n}}(\mathbf{y}_{k,i}) \langle \mathbf{n}, \mathbf{y}_{k,i} \rangle \mathbf{y}_{k,i}$$

for  $i = 1, \dots, L$  such that the vertex  $\mathbf{y}_{k,i}$  lies on the boundary  $\Gamma_k$ . These is an overdetermined system for the single unknown  $\alpha_k$  which we solve in the least-squares sense.

In Figure 6 and Figure 7, we visualized the boundaries fitted in accordance with the proposed method for both examples and for all noise levels applied. However, we

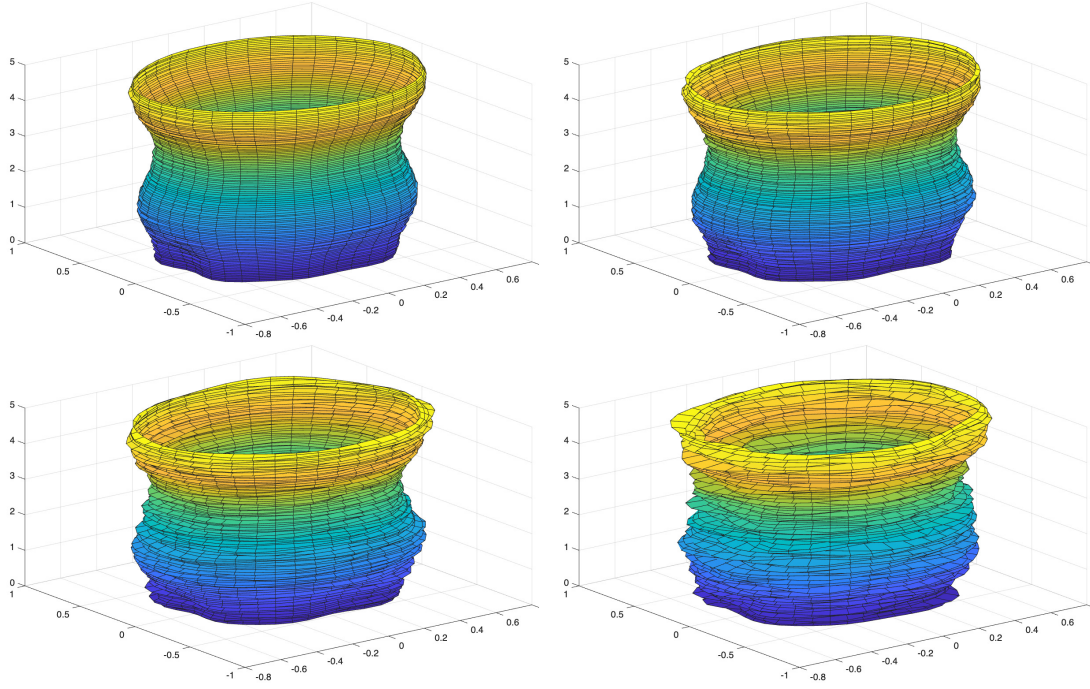


FIGURE 7. The reconstruction of the space-time tube in case of the second example with 0.25% random noise (top left), 0.5% random noise (top right), 1.0% random noise (bottom left), and 2.0% random noise (bottom right).

should mention that the computations in the  $(k + 1)$ -st step is always based on the prescribed domain  $\Omega_k^{\text{desired}}$ .

**4.5. Reconstructions of the melting temperature.** In case of the first example, the reconstructed melting temperature is found in Figure 8. The left plot shows the computed scaling factors which correspond to  $\dot{u}_m$ . The red curve corresponds to the noise level  $\delta = 0.1\%$ , the black one to the noise level  $\delta = 0.5\%$ , the blue one to the noise level  $\delta = 1\%$ , and the magenta one to the noise level  $\delta = 2\%$ . Especially the latter one oscillates quite a lot. However, if we integrate over time to obtain the melting temperature  $u_m$ , the fluctuations are significantly reduced.

We clearly can recognize the applied melting temperature  $u_m(t) = 1/20(t - 5/2)^2$  in the right plot of Figure 8. However, we observe that the discrepancy of the reconstructed melting temperature and the prescribed melting temperature grows as the time  $t$  increases. Moreover, the error of the reconstructions increases as the noise level increases as can be expected. Especially, we observe that the reconstruction of the

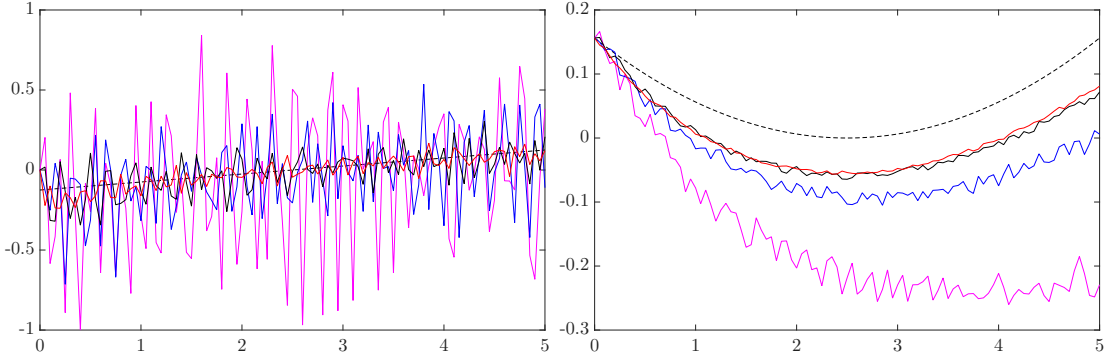


FIGURE 8. The reconstruction of the derivative  $\dot{u}_m(t)$  of the melting temperature (left) and the melting temperature  $u_m(t)$  (right) in case of the first example for the different noise levels: 0.25% noise – red, 0.5% noise – black, 1.0% noise – blue, and 2.0% noise – magenta. The true solution is indicated by the dashed black line.

melting temperature is not very useful for large time  $t$  in the case of the highest noise level.

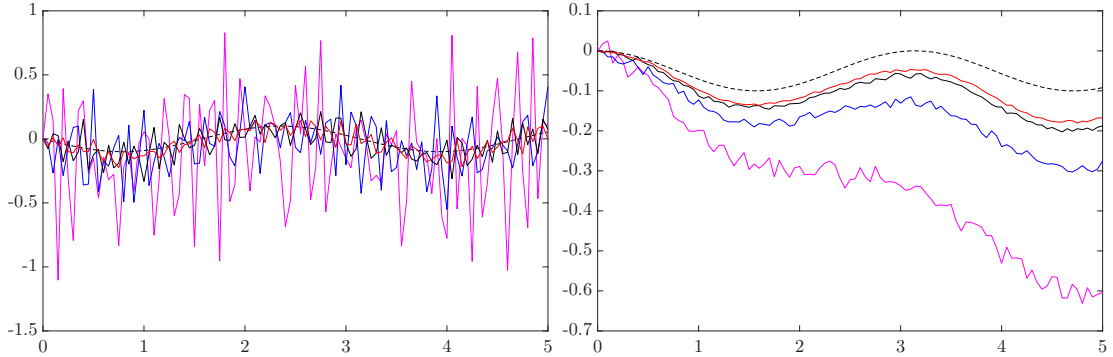


FIGURE 9. The reconstruction of the derivative  $\dot{u}_m(t)$  of the melting temperature (left) and the melting temperature  $u_m(t)$  (right) in case of the second example for the different noise levels: 0.25% noise – red, 0.5% noise – black, 1.0% noise – blue, and 2.0% noise – magenta. The true solution is indicated by the dashed black line.

Similar observations can be made in case of the reconstructions of the melting temperature in the second example, which are found in Figure 9. We likewise observe in the left plot of Figure 9 an increase of the oscillations in  $\dot{u}_m$  when the noise level increases, where the colour coding of the graphs is the same as for the first example. Nonetheless, the melting temperature  $u_m(t)$  itself is reasonably well reconstructed as can be seen in the right plot of Figure 9. But the reconstruction of the melting temperature for the highest noise level is again very inaccurate for larger time  $t$ .

## 5. CONCLUSION

In the present article, we considered the numerical solution of a Stefan problem, where the melting temperature varies over time. This happens in practical applications when the pressure in the external space changes during time for example. We provided a numerical algorithm to simulate such a transient Stefan problem that is based on finite elements defined on a moving mesh. We investigated in addition also the respective inverse problem – the reconstruction of the melting temperature from measurements of the evolving boundary. We demonstrated that this inverse problem can indeed be solved numerically, leading to reasonable reconstructions of the melting temperature. We presented different computations to validate the feasibility of the proposed approach.

## REFERENCES

- [1] D. Braess. *Finite Elements. Theory, Fast Solvers, and Applications in Solid Mechanics*. Cambridge University Press, Cambridge, 2nd edition, 2001.
- [2] S.C. Brenner and L.R. Scott. *The Mathematical Theory of Finite Element Methods*. Texts in Applied Mathematics. Springer, New York, NY, 3rd edition, 2008.
- [3] R. Brügger and H. Harbrecht. On the reformulation of the classical Stefan problem as a shape optimization problem. *SIAM Journal on Control and Optimization*, 60(1):310–329, 2022.
- [4] R. Brügger, H. Harbrecht, and J. Tausch. Boundary integral operators for the heat equation in time-dependent domains. *Integral Equations and Operator Theory*, 94:10, 2022.
- [5] J.W. Cooley and J.W. Tukey. An algorithm for the machine calculation of complex Fourier series. *Mathematics of Computation*, 19(90):297–301, 1965.
- [6] J. Crank. *Free and Moving Boundary Problems*. Clarendon Press Oxford, Oxford, 1984.
- [7] J. Crank and P. Nicolson. A practical method for numerical evaluation of solution of partial differential equations of the heat conduction type. *Mathematical Proceedings of the Cambridge Philosophical Society*, 43(1):50–67, 1947.
- [8] G.E. Fasshauer. *Meshfree Approximation Methods with MATLAB*. World Scientific, River Edge, 2007.
- [9] A. Friedman. Remarks on the maximum principle for parabolic equations and its applications. *Pacific Journal of Mathematics*, 8(2):201–211, 1958.
- [10] A. Friedman and D. Kinderlehrer. A one phase Stefan problem. *Indiana University Mathematics Journal*, 24(11):1005–1035, 1975.

- [11] R.M. Furzeland. A comparative study of numerical methods for moving boundary problems. *Journal of the Institute of Mathematics and its Applications*, 26(4):411–429, 1980.
- [12] S.C. Gupta. *The Classical Stefan Problem. Basic Concepts, Modelling and Analysis*, volume 45 of *North-Holland Series in Applied Mathematics and Mechanics*. Elsevier, Amsterdam, 2003.
- [13] M. Hadžić and S. Shkoller. Global stability and decay for the classical Stefan problem. *Communications on Pure and Applied Mathematics*, 68(5):689–757, 2014.
- [14] M. Hadžić and S. Shkoller. Well-posedness for the classical Stefan problem and the zero surface tension limit. *Archive for Rational Mechanics and Analysis*, 223(1):213–264, 2016.
- [15] S. Hofmann and J.L. Lewis.  $l^2$  solvability and representation by caloric layer potentials in time-varying domains. *Annals of Mathematics*, 144(2):349 – 420, 1996.
- [16] S. Kutluay, A.R. Bahadir, and A. Özdeş. The numerical solution of one-phase classical Stefan problem. *Journal of Computational and Applied Mathematics*, 81:135–144, 1997.
- [17] J. Lujano and J. Tausch. A shape optimization method for moving interface problems governed by the heat equation. *Journal of Computational and Applied Mathematics*, 390:113266, 2021.
- [18] A.M. Meirmanov. *The Stefan Problem*. Walter de Gruyter, Berlin, 1992.
- [19] M. Moubachir and J.-P. Zolésio. *Moving Shape Analysis and Control*. Chapman & Hall / CRC, Taylor & Francis Group, USA, 2006.
- [20] L.I. Rubinstein. *The Stefan Problem*, volume 27 of *Translation of Mathematical Monographs*. American Mathematical Society, Providence, Rhode Island, 1971. Translated from the Russian by A.D. Solomon.
- [21] B. Samar, M. Dambrine, H. Harbrecht, A. Desmedt, and Broseta D. Thickening, temperature and guest concentration of the meltwater layer growing over a slowly melting gas hydrate. *Chemical Engineering Science*, 320(A):122375, 2026.
- [22] J. Stefan. Über die Theorie der Eisbildung, insbesondere über die Eisbildung im Polarmeere. *Sitzungsberichte der Kaiserliche Akademie der Wissenschaften in Wien, Abteilung 2*, 98:965–983, 1889.
- [23] D.A. Tarzia. A bibliography on moving-free boundary problems for the heat-diffusion equation. The Stefan and related problems. *MAT Series A: Mathematical Conferences, Seminars and Papers*, 2, 1988.
- [24] A. Visintin. *Handbook of Differential Equations: Evolutionary Equations*, volume IV, chapter 8, pages 377–484. Elsevier, Amsterdam, 2008.
- [25] H. Wendland. *Scattered Data Approximation*. Cambridge University Press, Cambridge, 2004.
- [26] J.-P. Zolésio. *Identification de domaines par déformations*. PhD thesis, Université de Nice, 1979.

MARC DAMBRINE, UNIVERSITÉ DE PAU ET DES PAYS DE L'ADOUR, IPRA-LMA, UMR  
CNRS 5142, AVENUE DE L'UNIVERSITÉ, 64000 PAU, FRANCE

*Email address:* `marc.dambrine@univ-pau.fr`

HELMUT HARBRECHT, DEPARTEMENT MATHEMATIK UND INFORMATIK, UNIVERSITÄT  
BASEL, SPIEGELGASSE 1, 4051 BASEL, SCHWEIZ

*Email address:* `helmut.harbrecht@unibas.ch`